Manganese Oxidation Site in *Pleurotus eryngii* Versatile Peroxidase: A Site-Directed Mutagenesis, Kinetic, and Crystallographic Study[†,‡]

Francisco J. Ruiz-Dueñas,[§] María Morales,[§] Marta Pérez-Boada,[§] Thomas Choinowski,[||] María Jesús Martínez,[§] Klaus Piontek,[||] and Ángel T. Martínez*[,§]

Centro de Investigaciones Biológicas, CSIC, Ramiro de Maeztu 9, E-28040 Madrid, Spain, and Institute of Biochemistry, Swiss Federal Institute of Technology (ETH), Schafmattstrasse 18 (HPM), ETH Hönggerberg, CH-8093 Zürich, Switzerland

Received July 31, 2006; Revised Manuscript Received October 19, 2006

ABSTRACT: The molecular architecture of versatile peroxidase (VP) includes an exposed tryptophan responsible for aromatic substrate oxidation and a putative Mn^{2+} oxidation site. The crystal structures (solved up to 1.3 Å) of wild-type and recombinant *Pleurotus eryngii* VP, before and after exposure to Mn^{2+}, showed a variable orientation of the Glu36 and Glu40 side chains that, together with Asp175, contribute to Mn^{2+} coordination. To evaluate the involvement of these residues, site-directed mutagenesis was performed. The E36A, E40A, and D175A mutations caused a 60−85-fold decrease in Mn^{2+} affinity and a decrease in the Mn^{2+} oxidation activity. Transient-state kinetic constants showed that reduction of both compounds I and II was affected (80−325-fold lower k_{2app} and 10^3−10^4-fold lower k_{3app}, respectively). The single mutants retained partial Mn^{2+} oxidation activity, and a triple mutation (E36A/E40A/D175A) was required to completely suppress the activity (<1% k_{cat}). The affinity for Mn^{2+} also decreased (~25-fold) with the shorter carboxylate side chain in the E36D and E40D variants, which nevertheless retained 30−50% of the maximal activity, whereas similar mutations caused a 50−100-fold decrease in k_{cat} in the case of the *Phanerochaete chrysosporium* manganese peroxidase (MnP). Additional mutations showed that introduction of a basic residue near Asp175 did not improve Mn^{2+} oxidation as found for MnP and ruled out an involvement of the C-terminal tail of the protein in low-efficiency oxidation of Mn^{2+}. The structural and kinetic data obtained highlighted significant differences in the Mn^{2+} oxidation site of the new versatile enzyme compared to *P. chrysosporium* MnP.

Enzymatic oxidation of Mn^{2+} to Mn^{3+} is a unique characteristic of fungal peroxidases involved in lignin degradation (*1*), although it has also been reported in prokaryotic catalase−peroxidases (*2*). Enzyme oxidation of Mn^{2+} can also be produced indirectly, e.g., via the superoxide anion radical (*3*). Manganese peroxidase (MnP;[1] EC 1.11.1.13) was first discovered along with lignin peroxidase (LiP; EC 1.11.1.14) in the wood-rotting basidiomycete *Phanerochaete chrysosporium*, a model organism for lignin biodegradation studies. Both oxidoreductases have been extensively investigated since their discovery and subsequent cloning, including molecular characterization and structure−function relationship studies (*1*, *4*). These studies have been strongly stimulated by the biotechnological interest in ligninolytic enzymes as industrial biocatalysts for biotransformation of recalcitrant aromatic compounds including lignin (e.g., in biobleaching of paper pulp or even bioethanol production) (*5*).

Initially, LiP attracted more attention than MnP due to its ability to break down non-phenolic lignin model dimers, whereas the Mn-mediated action of MnP appeared to affect the phenolic units that represented only a small percentage of lignin (*6*). However, interest in MnP has increased in recent years since selective degradation of lignin has been demonstrated for fungi lacking LiP (*7*, *8*). These include *Pleurotus eryngii* (*8*), which produces a third family of ligninolytic peroxidases called "versatile peroxidases" (VP; EC 1.11.1.16) (*9*). Genes encoding VP isoenzymes have been cloned from *P. eryngii* (*10*, *11*) and *Bjerkandera adusta* (*12*). This new enzyme was able to directly oxidize Mn^{2+}, as MnP does, as well as high redox potential methoxybenzenes, like LiP, and phenolic aromatic substrates, as, for example, horseradish peroxidase (EC 1.11.1.7), in addition to substrates that cannot be directly oxidized by other peroxidases (*13*). It has also been demonstrated that VP is able to oxidize both phenolic and non-phenolic lignin model dimers (*14*).

The access to lignin in the plant cell wall is limited by the small size of molecular pores between cellulose microfibrils (*15*), which prevents penetration by the above

[†] This research was supported by EU contract QLK3-99-590 and Spanish projects BIO2002-1166 and BIO2005-02224. F.J.R.-D. thanks CSIC for an I3P contract and the Spanish Ministry of Education and Science (MEC) for a project contract, M.P.-B. thanks MEC for a FPI fellowship, and M.M. thanks CSIC for an I3P fellowship.

[‡] Atomic coordinates and structure factors for native VP* have been deposited in the Protein Data Bank (accession number 2BOQ).

* To whom correspondence should be addressed. Telephone: 34 918373112 (ext 4407). Fax: 34 915360432. E-mail: ATMartinez@cib.csic.es.

[§] Centro de Investigaciones Biológicas.

[||] Swiss Federal Institute of Technology.

[1] Abbreviations: ABTS, 2,2′-azino-bis(3-ethylbenzothiazoline-6-sulfonate); CCP, cytochrome *c* peroxidase; k_{obs}, pseudo-first-order rate constant; *k*, first-order rate constant; k_{app}, apparent second-order rate constant; k_{cat}, catalytic constant; K_D, equilibrium dissociation constant; K_m, Michaelis constant; LiP, lignin peroxidase; MnP, manganese peroxidase; PCR, polymerase chain reaction; PDB, Protein Data Bank; RMSD, root-mean-square deviation; SDS−PAGE, sodium dodecyl sulfate−polyacrylamide gel electrophoresis; VP, versatile peroxidase; VPI, compound I of VP; VPII, compound II of VP.

10.1021/bi061542h CCC: $37.00
Published on Web 12/14/2006

enzymes. Manganese is naturally present in wood, and the Mn^{3+} ion is a strong readily diffusable oxidizer (1.5 V redox potential in free form) which is able to penetrate the lignocellulose matrix. Moreover, the oxidizing power of Mn^{3+} is increased by the presence of unsaturated lipids, whose Mn^{3+}-mediated peroxidation generates free radicals (*16*). The potentiation of lignin degradation by redox mediators has been suggested for other ligninolytic oxidoreductases (*17*, *18*), but their relevance under natural conditions has still to be established. It is widely accepted, however, that Mn^{3+} is the natural mediator in lignin degradation by Mn^{2+}-oxidizing peroxidases (*19*). Studies on the mechanisms of enzymatic oxidation of Mn^{2+} are relevant both to understand the natural degradation of lignin and to develop new industrial biocatalysts.

The X-ray structure of MnP was determined shortly after that of LiP (*20*, *21*). Following early studies (*22*), the first evidence for the location of the Mn^{2+} oxidation site in MnP came from the crystal structure of the wild-type (nonrecombinant) enzyme isolated from Mn-containing cultures of *P. chrysosporium* (*21*, *23*). Site-directed mutagenesis in combination with homologous fungal expression was used to identify those amino acid residues contributing to Mn^{2+} oxidation (*24*−*28*). This information was confirmed by engineering Mn^{2+} oxidation sites into other heme peroxidases, although with much lower catalytic efficiencies than that of MnP (*29*−*31*). In the case of VP the broadening of heme proton NMR signals during titration with Mn^{2+} of the *P. eryngii* enzyme provided the first experimental evidence of Mn binding in proximity to the heme (*32*).

The VP cDNA (*10*) was expressed in *Escherichia coli* and reconstituted in vitro under conditions promoting disulfide bridge formation and heme incorporation, with a higher yield than previously reported for other secreted peroxidases (*33*). Recently, site-directed mutagenesis and *E. coli* expression, in combination with spectroscopic and crystallographic analyses, have been used to demonstrate long-range electron transfer from an exposed tryptophan residue in the oxidation of high redox potential aromatic compounds by VP (*34*, *35*) in a manner similar to that seen for LiP (*36*). From these results a revised catalytic cycle for oxidation of both Mn^{2+} and aromatic compounds by this peroxidase has been proposed (Figure 1). In the present study, the putative Mn^{2+} binding site was localized in the crystal structures (at near-atomic resolution) of wild-type and recombinant VP (VP*), which had been in contact with Mn. The contribution of the putative Mn ligands and other neighboring residues was evaluated by site-directed mutagenesis and kinetic and crystallographic characterization of the VP variants obtained.

MATERIALS AND METHODS

Heterologous Expression. Native (nonmutated) VP* protein and different site-directed variants were obtained by *E. coli* expression (*33*). The cDNA encoding the sequence of mature isoenzyme VPL of *P. eryngii* VP expressed in peptone-containing liquid cultures (allelic variant VPL2; GenBank AF007222) (*10*) was cloned in the expression vector pFLAG1 (International Biotechnologies Inc.), and the plasmid pFLAG1-VPL2 was used for site-directed mutagenesis using the polymerase chain reaction (PCR). *E. coli* DH5α was selected for plasmid propagation, whereas *E. coli*

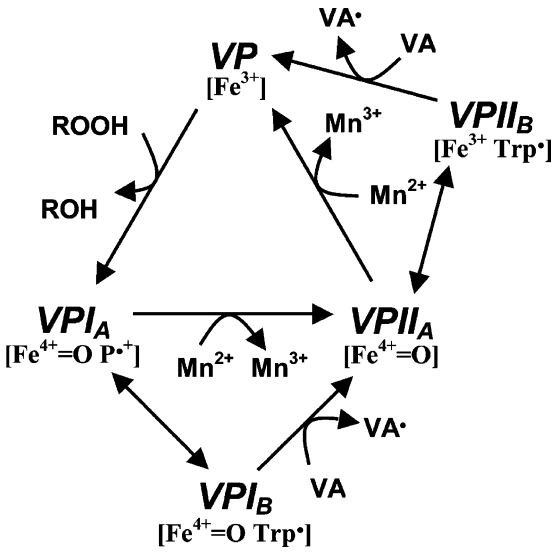

FIGURE 1: VP catalytic cycle (*35*). The scheme shows (i) the basic cycle involved in Mn^{2+} oxidation including two-electron oxidation of the resting peroxidase (VP, containing Fe^{3+}) by hydroperoxide to yield compound I_A (VPI_A, containing Fe^{4+}-oxo and the porphyrin cation radical), whose reduction in two one-electron steps results in the intermediate compound II_A ($VPII_A$, containing Fe^{4+}-oxo after the porphyrin reduction) and then the resting form of the enzyme, and (ii) the extended cycle including also compound I_B (VPI_B, containing Fe^{4+}-oxo and the Trp radical) and II_B ($VPII_B$, containing Fe^{3+} and the Trp radical) involved in oxidation of veratryl alcohol (VA) and other high redox potential aromatic compounds (VPI_B and $VPII_B$ are in equilibrium with VPI_A and $VPII_A$ respectively). Low redox potential aromatic compounds and dyes (like ABTS) are probably oxidized by both the A and B forms, but they are not included for simplicity.

W3110 was used for native and mutated cDNA expression. The VP* proteins obtained were reconstituted in vitro and purified as indicated below.

Site-Directed Mutagenesis. The mutations were introduced by PCR (*37*), using the expression plasmid pFLAG1-VPL2 as template and the QuikChange kit from Stratagene. For each mutation, both a direct and a reverse primer were designed complementary to opposite strands of the same DNA region. The changed codons for single mutants were GAA to GCA (E36A) or GAC (E36D), GAG to GCG (E40A) or GAC (E40D), GAC to GCC (D175A), and GCT to CGT (A173R). The double mutant E36A/E40A was obtained including the codons for both amino acids in the same primer (GAA to GCA and GAG to GCG). The triple mutant E36A/E40A/D175A was obtained as described for the double mutant but using plasmid pFLAG1-VPL2 (D175A) as template. Finally, the multiple mutant E36A/E40A/D175A/P327ter was obtained as described for the single ones but using plasmid pFLAG1-VPL2 (E36A/E40A/D175A) as template and direct and reverse oligonucleotides, introducing a termination codon (TAA) in substitution of the Pro327 codon, as primers. The mutated genes were completely sequenced using an ABI 377 automatic sequencer to ensure that only the desired single mutations occurred.

PCR reactions (50 μL final volume) were carried out in a Perkin-Elmer Gene Amp PCR System 240 using 10 ng of template DNA, 500 μM each dNTP, 125 ng of direct and reverse primers, 2.5 units of *Pfu*Turbo polymerase (Stratagene), and the manufacturer's buffer. Reaction conditions were as follows: (i) a "hot start" at 95 °C for 1 min; (ii) 18

cycles at 95 °C for 50 s, 55 °C for 50 s, and 68 °C for 10 min; and (iii) a final cycle at 68 °C for 10 min.

Enzyme Production and Purification. Native VP* and site-directed variants were produced in *E. coli* W3110 after transformation with the corresponding plasmids. Cells were grown for 3 h in Terrific broth (*38*), induced with 1 mM isopropyl β-D-thiogalactopyranoside, and grown for a further 4 h. The apoenzyme accumulated in inclusion bodies, as shown by sodium dodecyl sulfate−polyacrylamide gel electrophoresis (SDS−PAGE) (*39*), and was recovered using 8 M urea. Subsequently, in vitro folding was performed using 0.16 M urea, 5 mM Ca^{2+}, 20 μM hemin, 0.5 mM oxidized glutathione, 0.1 mM dithiothreitol, and 0.1 mg/mL protein concentration, at pH 9.5 (*33*). Active enzyme was purified by Resource-Q chromatography using a 0−0.3 M NaCl gradient (2 mL/min, 20 min) in 10 mM sodium tartrate (pH 5.5) containing 1 mM $CaCl_2$. Wild-type VP was obtained from filtrates of *P. eryngii* cultures, and its allelic variant VPL2 was purified as described elsewhere (*40*).

Spectroscopic Measurements. Electronic absorption spectra were recorded at 25 °C using a diode array Hewlett-Packard 8453 spectrophotometer. The concentrations of native VP* and site-directed variants were calculated from the absorption at 407 nm using an extinction coefficient of 150 mM^{-1} cm^{-1} (*10*). For spectroscopic characterization of the transient states in the VP catalytic cycle, 1 equiv of H_2O_2 was added to the resting enzyme in 10 mM sodium tartrate (pH 5), yielding compound I. Addition of 1 equiv of ferrocyanide to compound I yielded compound II (*25*).

Steady-State Enzyme Kinetics. Direct oxidation of Mn^{2+} was estimated by the formation of the Mn^{3+}•tartrate complex (ϵ_{238} 6500 M^{-1} cm^{-1}) using 0.1 M sodium tartrate (pH 5). Mn-independent activity on veratryl (3,4-dimethoxybenzyl) alcohol (veratraldehyde ϵ_{310} 9300 M^{-1} cm^{-1}) was estimated at pH 3.0, and those on 2,2′-azinobis(3-ethylbenzothiazoline-6-sulfonate) (ABTS; cation radical ϵ_{436} 29300 M^{-1} cm^{-1}) and Reactive Black 5 (ϵ_{598} 30000 M^{-1} cm^{-1}) were estimated at pH 3.5. All enzymatic activities were measured as initial velocities, taking linear increments (decreases in the case of Reactive Black 5) at 25 °C in the presence of 0.1 mM H_2O_2. Steady-state constants were calculated from oxidation of increasing substrate concentrations at 25 °C. Mean values and standard errors for the apparent affinity constant (Michaelis constant, K_m) and maximal enzyme turnover (catalytic constant, k_{cat}) were obtained by fitting the experimental measurements to the Michaelis−Menten model by double-reciprocal plots. Fitting of these constants to the normalized equation $v = (k_{cat}/K_m)[S]/(1 + [S]/K_m)$ yielded efficiency values (k_{cat}/K_m) with their corresponding standard errors.

Transient-State Enzyme Kinetics. Transient-state kinetic constants were measured at 25 °C (and 10 °C in some cases) using Bio-Logic stopped-flow equipment including a three-syringe module SFM300 synchronized with a J&M diode array detector and Bio-Kine software. Compound I formation was investigated by mixing the resting enzyme (1 μM final concentration) with increasing concentrations of H_2O_2 in 50 mM sodium tartrate (pH 5) under pseudo-first-order conditions, characterized by an excess of substrate, and followed at 397 nm (the isosbestic point of VP compounds I and II) to exclude interferences from eventual reduction of compound I. To investigate compound II formation, compound I was first prepared by mixing 4 μM resting enzyme with 1 equiv of H_2O_2 in 10 mM sodium tartrate (pH 5). After 2 s aging in a delay line, a ≥10-fold molar excess of Mn^{2+} in 50 mM (final concentration) sodium tartrate (pH 5) was added, and compound II formation was followed at 416 nm (the isosbestic point of VP compound II and resting enzyme). The first step to investigate compound II reduction consisted of production and reduction of compound I by premixing a solution of 4 μM enzyme and 4 μM ferrocyanide with 1 equiv of H_2O_2 in 100 mM sodium tartrate (pH 5). The mixture was incubated for 4 s, and compound II reduction was followed at 406 nm (the Soret maximum of resting enzyme) after mixing with different concentrations of Mn^{2+}, in 50 mM sodium tartrate (final concentration), pH 5. In all cases, the final concentration of enzyme was 1 μM. All kinetic traces exhibited single-exponential character from which pseudo-first-order rate constants were calculated.

Crystallization, Data Collection, and Crystal Structure Determination. Initial crystallization conditions for untreated VP* (after in vitro reconstitution), native VP* (treated with 50 mM $MnSO_4$ before crystallization), the VP* D175A variant (from site-directed mutagenesis), and wild-type VP from *P. eryngii*, corresponding to allelic variant VPL2 in all cases (*10*), were found by employing a commercial screen (Hampton Research) using the hanging drop vapor diffusion method and subsequently improved. Different crystallization conditions were finally selected to obtain single crystals of the different VP/VP* preparations, using a protein concentration of 8−9 mg/mL in 10 mM sodium citrate in all cases. For wild-type VP the protein solution was at pH 4, and 1.9 M ammonium sulfate and 6% PEG-400 in 0.1 M HEPES buffer (pH 7) were used. For the different VP* samples, the protein solution was at pH 5.5, with 16% PEG-8000 as precipitant, and 0.1 M zinc acetate in 0.1 mM sodium cacodylate (pH 6.5) was used. Some untreated VP* crystals were soaked for 3 h with 50 mM $MnSO_4$ before data collection.

Diffraction data were collected at the X06SA beamline of the Swiss Light Source (SLS) synchrotron at 100 K. Diffraction data were processed and scaled with the program package XDS/XSCALE (*41*). The two isomorphous crystal structures were solved by molecular replacement, applying the program AMORE (*42*). In all cases the crystal structure of LiP isoenzyme H2 (PDB entry 1QPA) was used as the search model. Refinement of the initial structures was performed with the program REFMAC from the CCP4 suite (*43*), and subsequent rounds of rebuilding using various omit difference maps resulted in well-defined structures. The statistics of crystallographic data collection, processing, and refinement are summarized in Table 1.

RESULTS

Mn Oxidation Site in VP Crystal Structures. The crystal structures of recombinant, before and after exposure to Mn, and wild-type VP (isoenzyme VPL) have been solved with different resolutions (up to 1.3 Å) and a different Mn content (Table 1). The quality of the electron density for native VP* is shown in Figure 2. VPL shows the highest amino acid sequence identity with LiP isoenzymes H2 (60% identity) and H8 (58% identity), followed by MnP1 (55% identity) and *Coprinus cinereus* peroxidase (49% identity). After C_α

Table 1: Data Collection and Processing and Refinement Statistics of Crystal Structures of Untreated VP* (Immediately after *E. coli* Expression and in Vitro Reconstitution), Native VP* (Treated with Mn^{2+}), D175A Variant, and Wild-Type VP (from *P. eryngii* Culture)

	untreated VP*	native VP*	D175A	wild-type VP
data collection and processing				
beamline	DESY	SLS/X06SA	SLS/X06SA	DESY
T (K)	100	100	100	100
space group	$P4_3$	$P4_3$	$P4_3$	$P2_12_12_1$
unit cell, *a* (Å)	63	63	63	73
unit cell, *b* (Å)	63	63	63	93
unit cell, *c* (Å)	98	98	98	113
resolution range (Å)	1.81−40	1.33−65	2.11−40	2.75−50
completeness (%)	96.1	99.6	97.6	93.7
R_{sym} (%)	5.6	8.6	8.4	11.2
I/σ	11.9	10.4	9.1	11.3
refinement				
resolution range (Å)	1.84−40	1.33−60	2.11−40	2.8−40
R_{cryst} (%)	18.8	15.9	16.0	18.8
bond RMSD (Å)	0.015	0.016	0.017	0.028
molecules	1	1	1	2
residues	1−318	1−319	1−316	1A−316A + 1B−316B
heteroatoms	2 Ca^{2+}	2 Ca^{2+}, 5 Zn^{2+}, 1 Mn^{2+}	2 Ca^{2+}, 3 Zn^{2+}	4 Ca^{2+}, 2 Mn^{2+}
cofactor	1 heme	1 heme	1 heme	2 hemes

fitting the VP* crystal structure (PDB entry 2BOQ) showed the lowest root-mean-square deviations (RMSD) of C_α atoms with the LiP-H2 crystal structure (only 0.82 Å from superimposition of 233 of the 319 VP amino acid residues) followed by the crystal structures of MnP (2.20 Å from only 170 residues superimposed), *C. cinereus* peroxidase (2.67 Å from 276 residues superimposed), and LiP H8 (2.91−2.95 Å from 252 residues superimposed) (PDB entries 1QPA, 1MNP, 1ARX, and 1LGA/1LLP, respectively). The mean *B* value of the native VP* was 19.9 $Å^2$, the manganese *B* value was 31.7 $Å^2$, and the occupancy was estimated to be 1.0. For wild-type VP the overall *B* value was 27.7 $Å^2$. The two manganese ions of the two wild-type VP molecules in the asymmetric unit had temperature factors of 38.1 and 37.8 $Å^2$, and in both cases an occupancy of 1.0 was used during refinement. The main differences between LiP-H2, used as reference in molecular replacement, and the VP structures concerned the C-terminal tail, which is four amino acids shorter in VP, and the loop formed by LiP residues 58−63, which is absent from VP. Concerning the heme pocket and substrate binding sites, the most important difference concerns the absence of a Mn binding site in the LiP isoenzymes that have asparagine and alanine residues at the positions occupied by the Mn ligands Asp175 and Glu36 in the VP metal binding site described below. Although the VP crystal structures solved at high resolution corresponded to nonglycosylated protein expressed in *E. coli*, differences in glycosylation are to be expected in comparison to LiP. Among the two residues being O-glycosylated in LiP-H2, that homologous to LiP-H2 Ser334 is absent from VP (because of its shorter C-terminal tail) and the second one (VP Ser331 homologous to LiP-H2 S332) is in fact the last C-terminal amino acid. On the other hand, the only N-glycosylated residue in LiP-H2 (Asn257) is conserved in VP (as Asn250), but no attempts were made to build carbohydrate moieties in the wild-type VP structure due to the low quality of the electron density in this region and the limited resolution.

As other heme peroxidases, VP has a rather globular shape with the heme cofactor occupying the interior. The heme pocket is connected to the protein surface by a channel located near the heme pyrroles A and B (see Figure 3A for pyrrole nomenclature) that provides access for H_2O_2 to react with the heme iron yielding compound I (see Figure 1). A second access channel exists in VP, providing access to the putative Mn^{2+} oxidation site as described below.

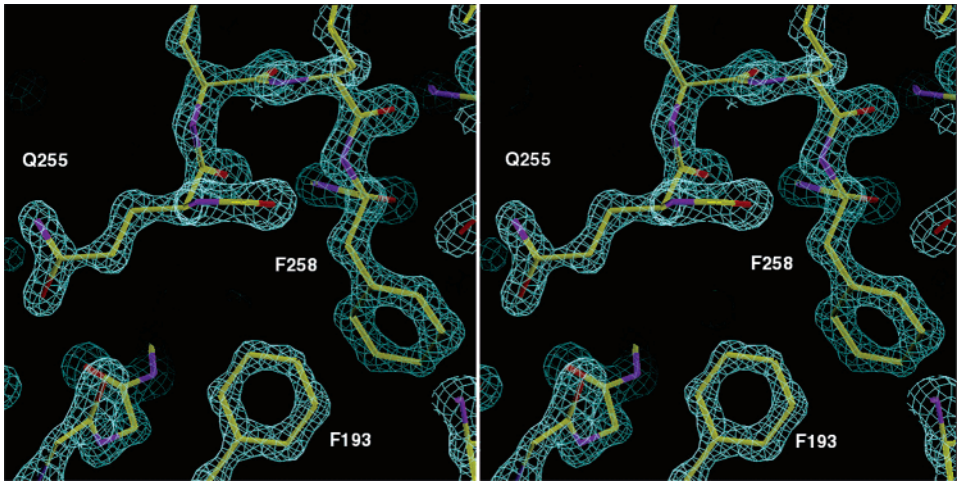

FIGURE 2: Stereoview of a representative electron density map [$(2F_o - F_c)\exp(i\alpha_c)$], contoured at a 3$\sigma$ level, of native VP* (PDB entry 2BOQ). A turn of the polypeptide in the region of Gln255 to Phe258 is shown, and Phe193 is also depicted.

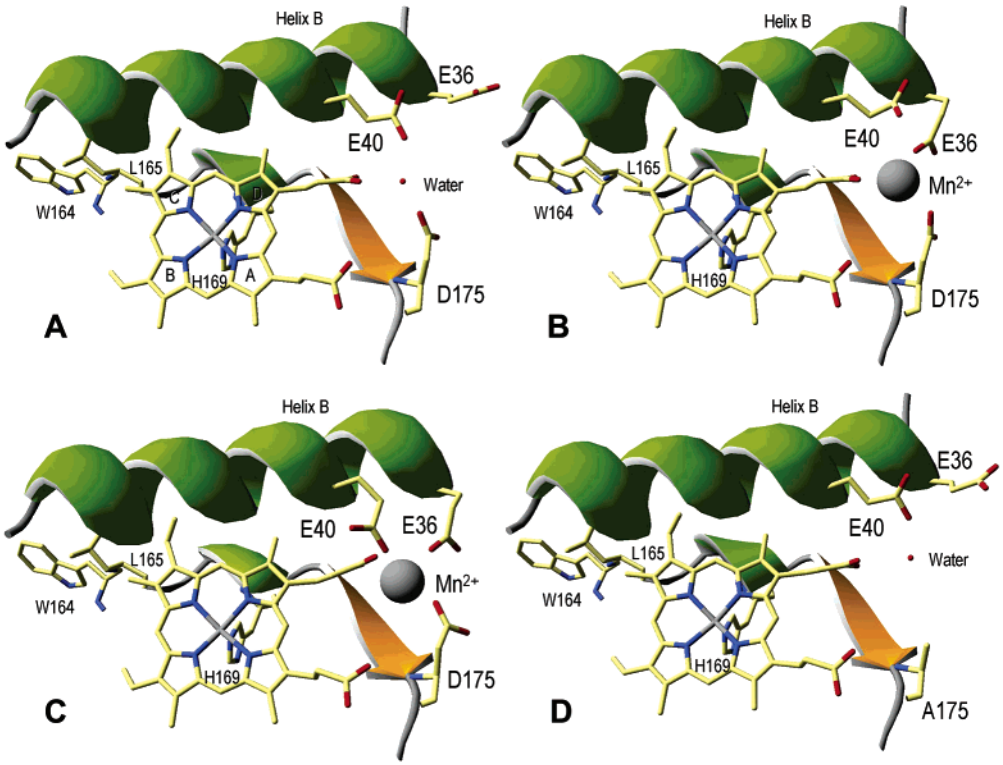

FIGURE 3: Axial views of the heme region including the putative Mn^{2+} binding site in VP* crystal structures. (A) Untreated native VP* after in vitro reconstitution. (B) Native VP* treated with Mn^{2+}. (C) Wild-type VP from the *P. eryngii* culture. (D) D175A variant treated with Mn^{2+}. The putative Mn^{2+} binding site in wild-type VP appeared to be formed by the carboxylates of Glu36, Glu40, and Asp175 and the heme internal propionate (at 2.17, 2.20, 2.06, and 2.22 Å from the metal, respectively), whereas only the Glu36 and Asp175 carboxylates and the internal propionate seemed to be involved in Mn^{2+} coordination in native VP*, and the site was occupied by a water molecule in the untreated VP* and D175A variant. Other residues relevant for VP activity (*35*), namely, His169 acting as a heme iron ligand, exposed Trp164 involved in aromatic substrate oxidation, and Leu165 contributing to electron transfer from Trp164 to the methyl of pyrrole C, are also included. Mn^{2+} is shown as a van der Waals sphere.

Figure 3 shows schematic axial views of the VP heme region, including the site where Mn^{2+} would be oxidized via the heme propionate D, as found in the crystal structures of VP just after its in vitro reconstitution (Figure 3A), and of the same enzyme after exposure to Mn^{2+} (Figure 3B). No Mn^{2+} was observed in VP* crystals soaked with $MnSO_4$. However, VP* treatment with Mn^{2+} before crystallization resulted in incorporation of one Mn^{2+} ion, which was located at 2.1 Å from the carboxylate of heme propionate D (Figure 3B). Whereas in this crystal structure the Glu36 and Asp175 side chains were oriented toward the Mn^{2+} ion at distances of 1.8 and 3.1 Å, respectively, a solvent molecule occupies the position of Mn^{2+} in the crystal structure of VP*, which had never been exposed to Mn during its production (Figure 3A). The side chain of Glu36 in this Mn-depleted structure was displaced with respect to its position in Figure 3B, pointing toward the opening of the Mn^{2+} access channel.

The Mn^{2+} oxidation site in crystals of wild-type VP purified from cultures of *P. eryngii* differed from that of VP*, the latter being a nonglycosylated protein produced in *E. coli* and reconstituted in vitro. Although the wild-type VP structure was solved at considerably lower resolution than those of VP*, the corresponding electron density map showed the presence of manganese at the putative oxidation site coordinated by the carboxylates of Glu36, Glu40, and Asp175 and heme propionate D (Figure 3C). The three amino acid side chains in the wild-type VP crystal structure point toward the position of Mn^{2+}, which is only 0.7 Å from the position of Mn^{2+} in 2BOQ, after superimposing both structures.

Site-Directed VP Variants: Steady-State Kinetics.* Six VP* variants were obtained by incorporating single mutations at the above-mentioned Glu36, Glu40, and Asp175 residues as well as at the Ala173 position. In addition to the six single variants, three VP* multiple variants were constructed, combining mutations at Glu36, Glu40, and Asp175 as well as at Pro327 in the C-terminal tail. Comparison of the resting state and compound I and II spectra for the different variants and native VP* showed that the mutations had not caused any substantial electronic changes in the heme environment. Table 2 shows the steady-state kinetic constants for oxidation of Mn^{2+}, veratryl alcohol, and Reactive Black 5 by the different variants, compared with native VP* (constants for oxidation of ABTS are provided as Supporting Information, Table S1). As expected, the single and multiple mutations mainly affected Mn^{2+} oxidation, and changes in the kinetic constants for the other substrates were always small and generally bordering on significance.

Removal of the side-chain carboxylate from only one of the three acidic residues (aspartate/glutamate to alanine mutations) resulted in a 250−1250-fold decrease of catalytic efficiency (k_{cat}/K_m) for Mn^{2+} oxidation. Although some reduction of k_{cat} (3−20-fold) was observed, the most important effect of these mutations was the increase of K_m (60−85-fold). This indicates that the Mn^{2+} oxidation site in VP is much less efficient in binding the cation when one of the three carboxylates is removed. Even when oxidation is

Table 2: Steady-State Kinetic Constants of Single and Multiple VP* Variants and Native VP* (Isoenzyme VPL), K_m (mM), k_{cat} (s^{-1}), and k_{cat}/K_m (mM^{-1} s^{-1}), for Oxidation of Mn^{2+}, Veratryl Alcohol (VA), and Reactive Black 5 (RB5)[a]

		VP*	E36A	E40A	D175A	E36D	E40D
Mn^{2+}	K_m	0.189 ± 0.016[b]	13.84 ± 0.87	11.26 ± 0.98	16.10	4.98 ± 0.31	4.91 ± 0.28
	k_{cat}	298 ± 9	85 ± 5	15 ± 0.5	32 ± 1	103 ± 0	145 ± 2
	k_{cat}/K_m	1600 ± 100	6.2 ± 0.2	1.3 ± 0.1	1.9 ± 0.1	20.7 ± 1.3	29.6 ± 1.2
VA	K_m	2.75 ± 0.25	4.32 ± 0.19	3.45 ± 0.24	2.30 ± 0.13	3.65 ± 0.25	4.12 ± 0.16
	k_{cat}	8.0 ± 0.4	12.8 ± 0.2	8.5 ± 0.3	22.0 ± 0.3	13.8 ± 0.4	9.5 ± 0.2
	k_{cat}/K_m	3.0 ± 0.1	3.0 ± 0.1	2.5 ± 0.1	9.6 ± 0.4	3.8 ± 0.2	2.3 ± 0.1
RB5	K_m	0.003 ± 0	0.004 ± 0	0.002 ± 0	0.002 ± 0	0.001 ± 0	0.001 ± 0
	k_{cat}	5.0 ± 0.0	7.7 ± 0.2	3.9 ± 0.1	7.2 ± 0.2	6.5 ± 0.4	5.0 ± 0.2
	k_{cat}/K_m	1780 ± 20	2100 ± 70	1800 ± 60	3170 ± 170	6150 ± 120	4330 ± 710

		A173R	E36A/E40A	E36A/E40A/D175A	E36A/E40A/D175A/P327ter[c]
Mn^{2+}	K_m	0.417 ± 0.021	46.86 ± 2.46	76.40 ± 3.89	69.97 ± 13.35
	k_{cat}	467 ± 24	5 ± 0	2 ± 0	2 ± 0
	k_{cat}/K_m	1100 ± 10	0.1 ± 0.0	0 ± 0	0 ± 0
VA	K_m	2.03 ± 0.11	3.21 ± 0.20	3.37 ± 0.03	2.66 ± 0.18
	k_{cat}	8.0 ± 0.1	12.7 ± 0.3	10.3 ± 0.0	4.9 ± 0.3
	k_{cat}/K_m	4.1 ± 0.2	3.9 ± 0.2	3.1 ± 0	1.9 ± 0.1
RB5	K_m	0.001 ± 0	0.003 ± 0	0.002 ± 0	0.001 ± 0
	k_{cat}	3.3 ± 0.2	5.2 ± 0.1	5.5 ± 0.4	4.4 ± 0.0
	k_{cat}/K_m	2280 ± 130	1980 ± 40	3560 ± 280	4270 ± 210

[a] Reactions at 25 °C in 0.1 M tartrate (pH 5 for Mn^{2+}, pH 3 for veratryl alcohol, and pH 3.5 for Reactive Black 5). [b] Lower K_m (0.037 ± 0.002 mM) when estimated as Mn-mediated oxidation of 2,6-dimethoxyphenol. [c] Quadruple variant with shortened C-terminal tail (by substituting the Pro327 codon by a termination codon). Means and 95% confidence limits of replicate assays.

saturated by increasing substrate concentration, the maximum turnover of all three variants is partially impaired.

The influence of the geometry of the Mn^{2+} oxidation site was investigated with the E36D and E40D variants, where the amino acid side chains were reduced in length by one methylene group. Substrate binding by these variants was better than found for the corresponding alanine variants, but the K_m values still remained 25-fold higher than those of native VP*. The two aspartate variants showed similar activities, which were only 2−3-fold lower than found for native VP*, indicating that electron transfer to heme (at high substrate concentration) is only slightly impaired.

When the three carboxylates were simultaneously removed in the triple variant E36A/E40A/D175A, the catalytic efficiency was practically zero (below 0.05 s^{-1} M^{-1}). At very high Mn^{2+} concentrations (near the molar range) this variant still showed some residual activity, although with a turnover of only 2 s^{-1}.

In the *P. chrysosporium* MnP crystal structures (PDB entries 1MNP and 1YYD) Arg177 is present near Asp179, which is involved in Mn^{2+} oxidation, whereas Ala173 occupies this position in the VP structure. To test if an arginine residue at this position could improve Mn^{2+} oxidation by VP, a variant containing the A173R mutation was produced. However, the presence of the arginine residue, although it slightly increased the Mn^{2+} oxidation turnover, resulted in a lower (1.5-fold) catalytic efficiency due to a decrease in affinity for Mn^{2+}.

The exact position of the C-terminal tail could not be established in the VP* crystal structures due to its high mobility, but there is potential for it to be located near the Mn^{2+} binding site. To investigate whether it could participate in Mn^{2+} binding at high substrate concentrations, an additional mutation was introduced in the triple variant that removed the last five residues of VP by substituting the Pro327-encoding triplet by a termination codon. However, the quadruple variant (E36A/E40A/D175A/P327ter) showed the same kinetic constants of the triple variant.

Table 3: Transient-State Kinetic Constants of Single and Multiple VP* Variants Compared with Native VP* (Isoenzyme VPL): Apparent Second-Order Rate Constants (mM^{-1} s^{-1}) of Compound I Formation (k_{1app}) by H_2O_2 and Compound I (k_{2app}) and II Reduction (k_{3app}) by Mn^{2+} [a]

	k_{1app}	k_{2app}	k_{3app}
VP*	3460 ± 70	≈36500[b] (≈13000)	3490 ± 80
E36A	3530 ± 90	194 ± 6	3.70 ± 0.30
E40A	3920 ± 30	451 ± 11	0.37 ± 0.04
D175A	4100 ± 70	113 ± 4	0.58 ± 0.05
E36D	3780 ± 30	1370 ± 20	13.70 ± 0.70
E40D	3530 ± 30	10400 ± 600 (3700 ± 110)	42.10 ± 4.70
A173R	3830 ± 40	≈26500[b] (≈9400)	794 ± 50
E36A/E40A	3730 ± 50	2.94 ± 0.03	0.02 ± 0
E36A/E40A/D175A	3930 ± 90	0.03 ± 0	0.01 ± 0
E36A/E40A/D175A/P327ter[c]	3830 ± 90	0.03 ± 0	0.01 ± 0

[a] Reactions at 25 °C in 50 mM sodium tartrate (pH 5) using 1 μM VP, final concentration, conducted as described in the text. [b] Approximate values at 25 °C of very rapid reactions, which could be estimated from the constants of reactions at 10 °C (the latter in parentheses). [c] Quadruple variant with shortened C-terminal tail (by substituting the Pro327 codon by a termination codon). Means and 95% confidence limits of replicate assays.

Transient-State Kinetics of VP Variants: Compound I Formation and Reduction.* The kinetic constants for formation and reduction of the transient states (compounds I and II) of the VP catalytic cycle (Figure 1) in the site-directed variants were estimated and compared with those of native VP*. Compound I formation was measured at 397 nm. In both native VP* and site-directed variants the observed pseudo-first-order rate constants (k_{1obs}), calculated from the kinetic traces, exhibited a linear dependence of the H_2O_2 concentration passing through the origin (data not shown). Fitting of k_{1obs} vs H_2O_2 concentration to a straight line yielded slope values corresponding to the apparent second-order rate

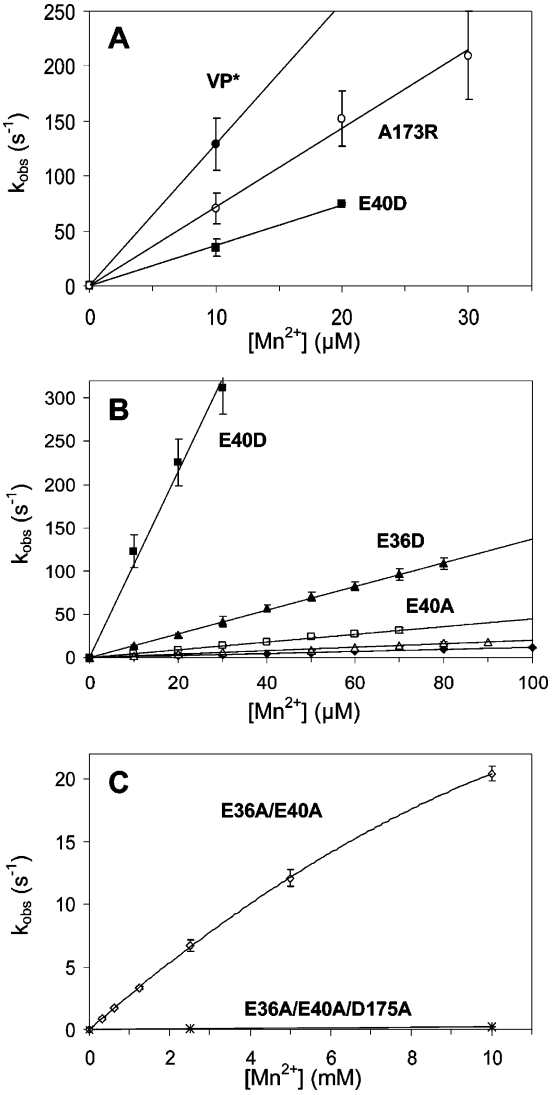

FIGURE 4: Kinetics of compound I reduction by Mn^{2+}. (A) Reactions of native VP* (isoenzyme VPL) (●) and the A173R (○) and VPL E40D (■) variants at 10 °C (reduction of native VP* and the A173R variant compound I was too fast at 25 °C). (B) Reactions of the single E40D (■), E36D (▲), E40A (□), E36A (△), and D175A (◆) variants at 25 °C. (C) Reactions of the multiple E36A/E40A (◇) and VPL E36A/E40A/D175A (×) variants at 25 °C. Note the different *x* and *y* scales used in the three graphs. The reaction mixtures contained 1 μM enzyme and 50 mM tartrate (pH 5). All kinetic traces displayed single-exponential character and were fitted to obtain k_{obs} values. Means and 95% confidence limits of replicate assays are shown.

constant for compound I formation (k_{1app}). The similar k_{1app} values obtained for native VP* and all of the site-directed variants (Table 3) confirmed that the mutations did not affect the formation of compound I by H_2O_2.

The single-electron reduction of VP compound I by Mn^{2+} was examined at 416 nm. All of the kinetic traces exhibited single-exponential character from which the pseudo-first-order rate constants (k_{2obs}) were calculated. Plots of k_{2obs} vs Mn^{2+} concentration were linear for native VP* and all of the single variants (Figure 4A,B), and an apparent second-order rate constant for compound I reduction (k_{2app}) was determined as the slope of a second-order plot (Table 3). By contrast, the VP* multiple variants showed saturation kinetics (Figure 4C), and first-order rate constants (k_2) and equilibrium dissociation constants (K_{D2}) for compound I reduction could be calculated by considering the process as a simple binding interaction between reactants according to eqs 1−3.

$$\mathrm{VPI} + \mathrm{Mn^{2+}} \overset{K_{D2}}{\rightleftharpoons} \mathrm{VPI{-}Mn^{2+}} \xrightarrow{k_2} \mathrm{VPII} + \mathrm{Mn^{3+}} \quad (1)$$

$$k_{2obs} = k_2/(1 + K_{D2}/[\mathrm{Mn^{2+}}]) \quad (2)$$

$$K_{D2} = [\mathrm{VPI}][\mathrm{Mn^{2+}}]/[\mathrm{VPI{-}Mn^{2+}}] \quad (3)$$

The apparent second-order rate constant k_{2app} (k_2/K_{D2}) for these variants was estimated by a nonlinear least-squares fit to eq 2 adapted as follows: $k_{2obs} = (k_2/K_{D2})[\mathrm{Mn^{2+}}]/(1 + [\mathrm{Mn^{2+}}]/K_{D2})$.

Compounds I of native VP* and the A173R variant oxidized Mn^{2+} so rapidly that it was necessary to estimate the k_{2app} at 10 °C and then extrapolate to 25 °C (after measuring E40D compound I reduction at both temperatures). The resulting k_{2app} values were similar for both enzymes (Table 3). Reduction of VP compound I by Mn^{2+} was strongly decreased by mutations at Glu36, Glu40, and Asp175, as shown by a decrease of 2 orders of magnitude in the k_{2app} values for the three alanine variants (Table 3). The decrease was of only 1 order of magnitude in the E36D variant, and surprisingly, reduction of compound I was only slightly affected when Glu40 was substituted by an aspartate (the E40D k_{2app} being of the same order of magnitude as that of native VP* and the A173R variant).

In the case of double mutants, k_{2app} values decreased by 4 orders of magnitude, and 6 orders of magnitude in the case of a triple mutation (Table 3). Comparison of the limiting first-order rate constants for reduction of compound I for the E36A/E40A (k_2 67 ± 2 s^{-1} and K_{D2} 23 ± 1 mM) and E36A/E40A/D175A (k_2 1.1 ± 0.1 s^{-1} and K_{D2} 40 ± 8 mM) variants revealed that k_2 was more affected (60-fold decrease) than K_{D2} (less than 2-fold increase) when the third Mn ligand was removed. Removal of the C-terminus in the E36A/E40A/D175A/P327ter variant did not affect the compound I reduction kinetics.

Transient-State Kinetics of VP Variants: Compound II Reduction.* The one-electron reduction of VP* compound II to the resting enzyme by Mn^{2+} was followed at 406 nm. Plots of pseudo-first-order rate constants (k_{3obs}) vs Mn^{2+} concentration exhibited a hyperbolic behavior, the rates saturating with increasing Mn^{2+} concentration for both native VP* and variants (Figure 5). Compound II reduction can be explained by eqs 4−6, k_3 and K_{D3} being its first-order rate constant and equilibrium dissociation constant, respectively.

$$\mathrm{VPII} + \mathrm{Mn^{2+}} \overset{K_{D3}}{\rightleftharpoons} \mathrm{VPII{-}Mn^{2+}} \xrightarrow{k_3} \mathrm{VP} + \mathrm{Mn^{3+}} \quad (4)$$

$$k_{3obs} = k_3/(1 + K_{D3}/[\mathrm{Mn^{2+}}]) \quad (5)$$

$$K_{D3} = [\mathrm{VPII}][\mathrm{Mn^{2+}}]/[\mathrm{VPII{-}Mn^{2+}}] \quad (6)$$

The apparent second-order rate constant of compound II reduction k_{3app} (k_3/K_{D3}) was calculated by a nonlinear least-squares fit to eq 5 adapted as follows: $k_{3obs} = (k_3/K_{D3})[\mathrm{Mn^{2+}}]/(1 + [\mathrm{Mn^{2+}}]/K_{D3})$.

Reduction of compound II was dramatically affected in all of the single variants, k_{3app} being 3−4 orders of magnitude

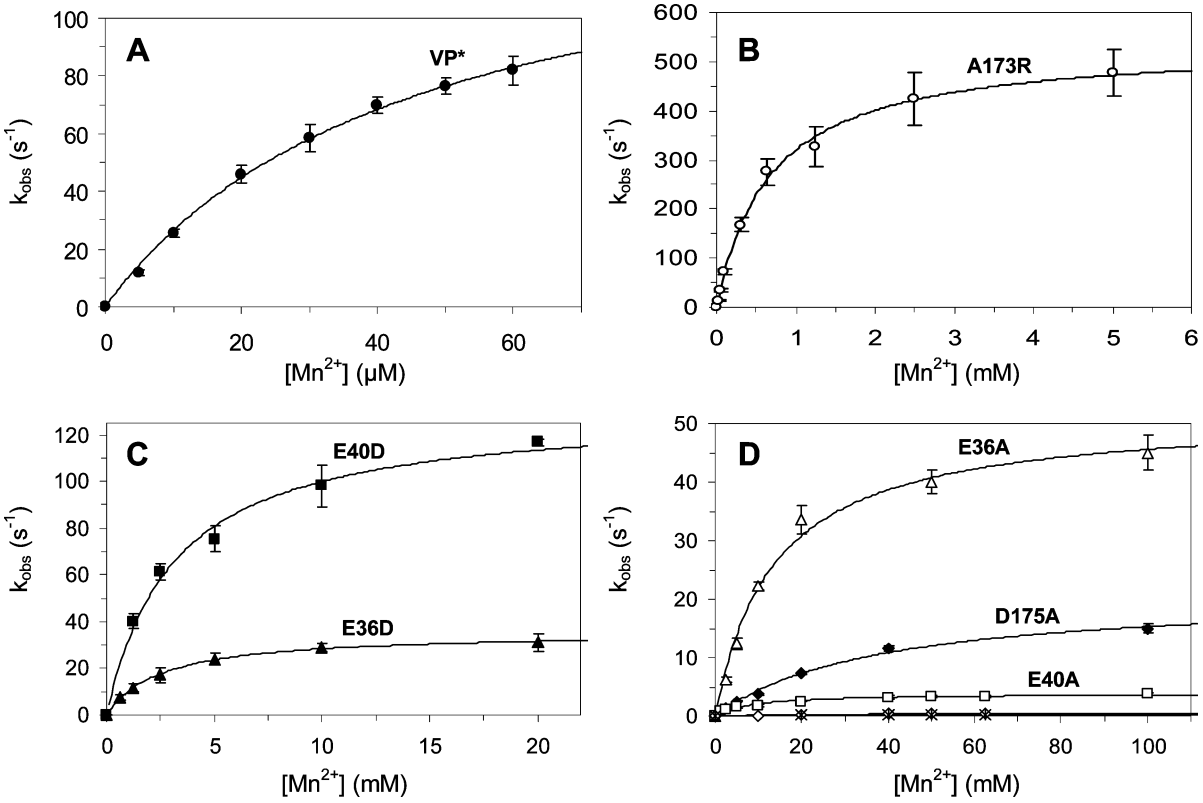

FIGURE 5: Kinetics of compound II reduction by Mn^{2+}. (A) VP* (isoenzyme VPL) (●). (B) A173R variant (○). (C) E40D (■) and E36D (▲) variants. (D) E36A (△), D175A (◆), E40A (□), E36A/E40A (◇), and E36A/E40A/D175A (×) variants. Note the different *x* and *y* scales used. Reactions were carried out at 25 °C using 1 μM enzyme and 50 mM tartrate (pH 5). All kinetic traces displayed single-exponential character and were fitted to obtain k_{obs} values. Means and 95% confidence limits of replicate assays are shown.

Table 4: Comparison of Transient-State Kinetic Constants for Compound II Reduction of Single and Multiple VP* (Isoenzyme VPL) Variants by Mn^{2+}: First-Order Rate Constants (k_3, s^{-1}) and Equilibrium Dissociation Constants (K_{D3}, mM)[a]

	k_3	K_{D3}
VP*	145 ± 7	0.045 ± 0.004
E36A	53 ± 4	14 ± 2
E40A	4.1 ± 0.2	11 ± 2
D175A	20 ± 1	35 ± 5
E36D	36 ± 2	2.7 ± 0.3
E40D	130 ± 6	3.1 ± 0.5
A173R	536 ± 14	0.68 ± 0.05
E36A/E40A	0.7 ± 0.0	35 ± 11
E36A/E40A/D175A	0.4 ± 0.0	28 ± 4.7
E36A/E40A/D175A/P327ter[b]	0.4 ± 0.0	38 ± 12

[a] Reactions at 25 °C in 50 mM sodium tartrate (pH 5) using 1 μM VP, final concentration, conducted as described in the text. [b] Quadruple variant with shortened C-terminal tail (by substituting the Pro327 codon by a termination codon). Means and 95% confidence limits of replicate assays.

lower for the three alanine variants and 2 orders of magnitude lower for the two glutamate variants (Table 3). The k_3 and K_{D3} values (Table 4) were in agreement with those estimated under steady-state conditions, indicating that compound II reduction is the limiting step at full saturation in the VP catalytic cycle (this agreement was more evident when the Mn^{2+} K_m was estimated by the Mn-mediated oxidation of 2,6-dimethoxyphenol). All of the single mutations caused a stronger effect on the Mn^{2+} K_{D3} (60−800-fold increase) than on the k_3 constant (1−35-fold decrease). The two Glu36 variants showed similar k_3 values, although the K_{D3} of the E36D variant was lower, as expected. However, the two Glu40 mutations caused very different effects. Whereas substitution by an alanine resulted in the lowest k_3 value, substitution by an aspartate resulted in a variant (E40D) with nearly the same k_3 as the native VP*. Finally, the A173R variant showed higher K_{D3} and k_3 values than those of native VP* for reduction of compound II, in agreement with the constants obtained under steady-state conditions.

Regarding the multiple variants, k_{3app} was decreased by 5 orders of magnitude in the E36A/E40A variant, the decrease extending to 6 orders of magnitude in the triple variant (a result similar to that observed for k_{2app}). As described for compound I reduction, comparison between the first-order rate constants for reduction of compound II of the E36A/E40A and E36A/E40A/D175A variants and those of the native enzyme (and single variants) revealed that the k_3 of the multiple variants showed a stronger perturbation than K_{D3} (Table 4). Finally, removal of the C-terminus did not affect compound II reduction constants with respect to the triple variant.

Crystal Structure of the D175A Variant. Figure 3D shows an axial view of the Mn^{2+} oxidation site in the crystal structure of the D175A variant. Removal of the D175 carboxylate, which caused a strong decrease in the ability of VP* to bind Mn^{2+} (85-fold higher K_m and 10^3-fold higher K_{D3}), resulted in the concomitant displacement of the Glu36 side chain which became parallel to that of Glu40 (which was slightly rotated with respect to native VP*) and the inclusion of a water molecule, at 2.8 Å from the propionate D, occupying the position of the metal ion in the Mn^{2+}-occupied site of the fungally produced enzyme (Figure 3B). Therefore, the Mn^{2+} binding site of the D175A variant of

VP* (Figure 3D) was basically similar to that of VP* untreated with Mn (Figure 3A).

DISCUSSION

Substrate Oxidation Sites in VP. Despite the fact that most lignin-degrading organisms secrete Mn^{2+}-oxidizing peroxidases (*5*, *44*) and significant differences in their catalytic properties have been reported (*4*, *45*), only those peroxidases from *P. chrysosporium* have been characterized in terms of their structure−function relationships (*1*). The work presented herein describes the investigation of Mn^{2+} oxidation by *P. eryngii* VP, a "hybrid" peroxidase that shares catalytic properties of MnP, LiP, and other peroxidases (*13*). We first demonstrated that oxidation of Mn^{2+} and other VP substrates takes place at different enzyme sites. The latter substrates included veratryl alcohol, the typical LiP substrate, and Reactive Black 5, a high redox potential dye that is not oxidized by MnP nor by LiP in the absence of veratryl alcohol. The existence of at least two oxidation sites in VP was first shown by noncompetitive inhibition between Mn^{2+} and Reactive Black 5 oxidation (*9*, *13*) and confirmed here by site-directed mutagenesis, resulting in several variants that were unable to oxidize Mn^{2+} but maintained their activity with the other substrates. In a similar way, VP mutants at the exposed Trp164, which oxidize Mn^{2+} but fail to act on high redox potential aromatic substrates, have been recently described (*35*).

Mn^{2+} Oxidation Site in VP Crystal Structures. Comparison of the crystal structures of wild-type VP from *P. eryngii* cultures, *E. coli*-expressed VP*, and its D175A variant showed differences in the position of the Glu36 and Glu40 side chains. Both chains pointed toward the opening of the Mn^{2+} access channel in untreated (Mn-free) VP*, and a similar orientation was observed in the D175A variant that was unable to bind Mn^{2+}. When Mn^{2+} was present, the side chain of Glu36 rotated inward, contributing to Mn^{2+} coordination together with Asp175 and heme propionate D, as found in wild-type VP from *P. eryngii* (exposed to Mn^{2+} in culture) and VP* treated with Mn^{2+}. In the wild-type VP crystals, the Glu40 side chain also pointed toward the Mn^{2+} ion, the four carboxylates being at coordination distance. This disposition agrees with that observed in wild-type and recombinant MnP from *P. chrysosporium* crystallized in the presence of Mn^{2+}, where three homologous residues participate in metal coordination (*21*). It is interesting that VP* expressed in *E. coli* and reconstituted in vitro yielded crystals that diffracted to a very high resolution (1.3 Å for some of the variants) (*35*), while the wild-type VP crystals diffracted only to a rather low resolution (about 2.8 Å). The reason might be a microheterogeneity of the protein samples caused by a variable glycosylation of the enzyme produced by the fungus (Piontek et al., unpublished results).

In *P. chrysosporium* MnP, no differences in the Mn^{2+} oxidation site were observed between wild-type and recombinant enzyme crystals (*21*, *23*). However, most probably this is because the MnP* used was obtained from *P. chrysosporium* (homologous) expression, whereas *E. coli* expression followed by in vitro reconstitution was used for VP*. In addition to eukaryotic expression systems (*46*, *47*), *E. coli* expression has also been used with MnP* (*48*, *49*), but no crystal structures have been reported.

Site-Directed Mutagenesis of Acidic Residues at the Mn Binding Site. To investigate how much the residues mentioned above were involved in binding, as well as other aspects of Mn^{2+} oxidation, nine VP* site-directed variants were produced. The kinetic constants of the E36A, E40A, and D175A variants revealed that the three acidic residues participate in both Mn^{2+} binding and oxidation, but they are not involved in oxidation of other high or low redox potential VP substrates. These include ABTS that, according to previous results (*13*), most probably has two different binding sites in VP characterized by different oxidation efficiencies. However, none of them corresponds to the Mn^{2+} oxidation site described herein. In a similar way, MnP compound I can oxidize phenols and dyes at a site that, as shown for VP, is different from that involved in Mn^{2+} oxidation (*24*, *25*).

In spite of the differences between the Glu40 side-chain position in wild-type VP and VP* crystals, which caused some doubts about its contribution to Mn^{2+} binding, this glutamate provides the highest contribution (as revealed when substituted by an alanine) to Mn^{2+} oxidation under steady-state conditions, as well as to compound II reduction under transient-state conditions. The same has been shown for MnP (*50*), although it had been initially suggested that Glu39 (homologous to VP Glu40) is less important than Glu35 and Asp179 at the Mn^{2+} binding site of this peroxidase (*28*). A MnP has been reported from *Ganoderma* species (*51*) that has only two acidic residues at the putative Mn binding site (GenBank BAA88392, ABB77244, and ABB77243). Its catalytic properties should be investigated in more detail, since sequence alignment (*4*) showed that it contains a tryptophan residue homologous to VP Trp164 (or LiP Trp171) involved in aromatic substrate oxidation (*35*, *36*).

The first site-directed mutagenesis studies of *P. chrysosporium* MnP showed that reduction of compound II by Mn^{2+} was lowered by mutations at the binding site (*24*, *25*). Reduction of both VP compounds I (80−320-fold lower k_{2app}) and II (10^3−10^4-fold lower k_{3app}) was affected by removing the side-chain carboxylates of Glu36, Glu40, and Asp175, as also shown for MnP (*28*, *50*). Not only binding but also the Mn^{2+} oxidation turnover was affected in these VP* variants. However, the decrease in VP* catalytic efficiency for the oxidization of Mn^{2+} was much lower than found in two similar MnP site-directed variants (E40A and D175A) (*25*, *28*, *50*). This is due to differences in k_{cat}, which decreased from around 300 s^{-1} in both native enzymes to 15−85 s^{-1} in the VP variants and only to 1−3 s^{-1} in the MnP variants. In fact, removal of the three carboxylates (in the E36A/E40A/D175A variant) was required to lower the VP* catalytic activity to similar levels. The above differences were also observed in transient-state measurements for reduction of VP compounds I and II, where the decreases were smaller than those found in MnP. Estimation of first-order rate constants for compound II reduction (those of compound I are too fast to be measured) showed that the above mutations strongly increased the dissociation constant (300−1000-fold) but only slightly affected k_3 (2−30-fold decrease), whereas a strong decrease in k_3 (100−1200-fold) was observed in the corresponding MnP variants (*25*, *28*, *50*).

Differences with *P. chrysosporium* MnP were also evident when the two glutamate residues at the Mn^{2+} oxidation site

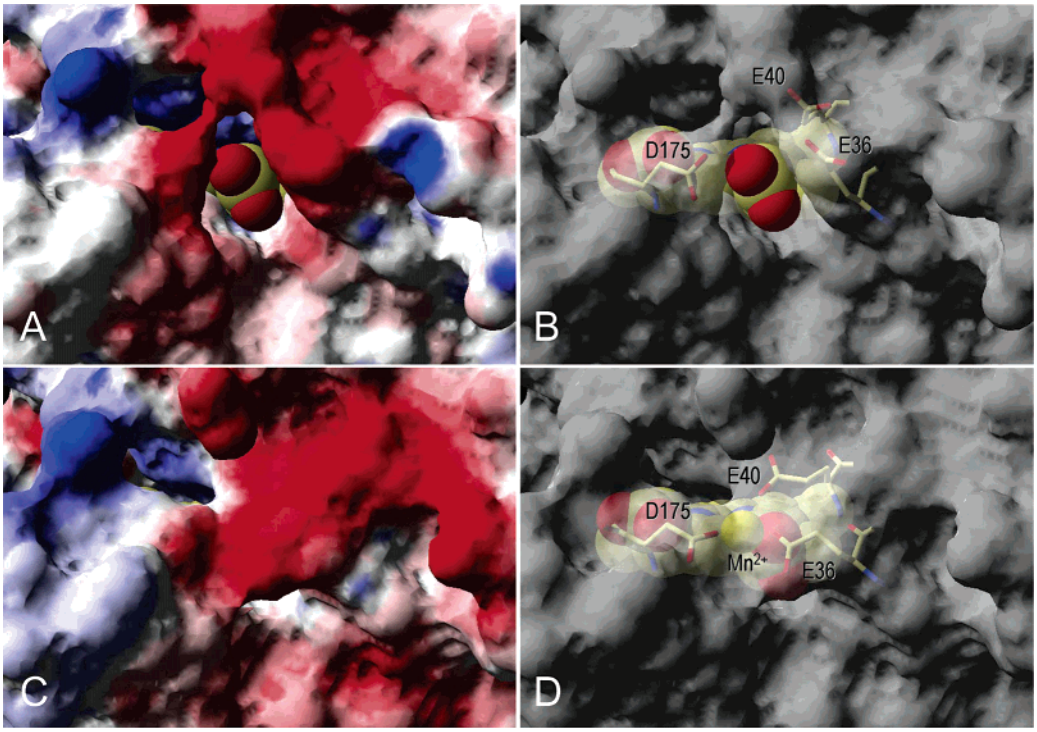

FIGURE 6: Solvent access surfaces at the Mn^{2+} oxidation site. (A, B) Mn channel open-gate conformation in crystals of untreated VP* before being in contact with Mn^{2+}, enabling access to heme propionate D. (C, D) Closed-gate conformation in crystals of wild-type VP. Surfaces show electrostatic charges in (A) and (C) or are partially transparent in (B) and (D) showing Glu36, Glu40, and Asp175 side chains, heme, and Mn^{2+}. Heme atoms and Mn^{2+} ion are shown as van der Waals spheres.

were substituted by aspartates in single variants. It has been reported that shortening the side chains of these residues by one methylene resulted in a 45−90-fold decrease of MnP k_{cat} (*25*, *50*), whereas only a 2−3-fold lower k_{cat} was found for the VP variants. The same tendency was observed in the first-order rate constant for compound II reduction (k_3) in the single variants; these showed 40−120-fold lower values in the case of MnP but only a 1−4-fold decrease in the case of VP.

Other Site-Directed Mutations near the VP Mn Binding Site. Another difference between MnP and VP concerns the residue located two positions before the aspartate involved in Mn^{2+} binding. It has been suggested that Arg177 in MnP would contribute to a proper orientation of the Glu35 side chain, its substitution by alanine decreasing Mn^{2+} binding (18-fold higher K_m) (*26*). Surprisingly, *P. eryngii* VP has an alanine at this position (as found in LiP), and its substitution by an arginine in the A173R variant resulted in a slightly lower efficiency in oxidizing Mn^{2+}. The analysis of the transient-state kinetic constants revealed that this was the result of two opposite effects, the increase in Mn^{2+} oxidation by the A173R variant compound II (3.7-fold higher k_3) and the decrease in the stability of enzyme-bound Mn^{2+} (a 15-fold higher dissociation constant). A characteristic of typical MnP from *P. chrysosporium* and other white-rot fungi is the presence of the above conserved arginine residue (MnP Arg177) together with a longer C-terminal tail, which seems to be displaced away from the entrance of the Mn channel by the arginine side chain (*4*, *21*). A similar residue would not be required for Mn^{2+} oxidation by VP because of its shorter C-terminal end.

Recent crystallographic studies have shown a second weak metal binding site in MnP−Cd^{2+} complexes near the C-terminus that it has been suggested could be operative for Mn^{2+} oxidation under physiological conditions (*52*). The low but detectable Mn^{2+} oxidation activity of the VP* triple variant (E36A/E40A/D175A) could be explained by the presence of this C-terminal oxidation site. This possibility was ruled out by a quadruple variant (E36A/E40A/D175A/P327ter), which showed the same steady-state and transient-state kinetic constants as the triple variant with the intact C-terminal tail. This agrees with NMR information during VP* titration with Mn^{2+} (*32*), which showed a maximal broadening of the signals corresponding to those heme protons closer to the Mn binding site, indicating that a second Mn^{2+} binding site does not exist at the vicinity of the heme. In fact, the low k_{2app} values obtained for these VP variants are similar to those reported for the residual Mn^{2+} oxidation activity found in LiP, which lacks a specific binding site for this ion (*53*).

Manganese Channel in VP. The side chains of Glu36 and Glu40 occupied different positions in the wild-type and recombinant VP crystal structures obtained. We postulate that the position in untreated VP* (and its D175A variant) corresponds to an "open-gate" conformation adopted in the absence of Mn^{2+} (or when the metal does not bind the enzyme due to mutation) (Figure 6A,B). The conformation in which the two glutamate side chains point toward the Mn^{2+} ion (found in wild-type VP) corresponds to the "closed-gate" conformation (Figure 6C,D), characteristic of the naturally folded enzyme from *P. eryngii* cultures. Opening of the homologous glutamate side chains was not observed in crystals of MnP grown in the presence of EDTA (*23*). However, a displacement of Glu35 and Glu39 side chains toward the opening of the Mn channel, similar to that found in VP crystals, was shown in crystals of a MnP variant that

does not bind Mn^{2+} (*23*), and more recently in native MnP, after removal with oxalate of the metal ion from MnP−Sm^{3+} crystals (*52*).

We were able to solve the VP* structure at high resolution using crystals grown in the presence of Zn^{2+}, but we experienced difficulties in crystallizing VP in the presence of Mn^{2+} (the crystals were unstable). This contrasted with MnP studies, where Mn^{2+} was reported to contribute to the stability of the crystals (*21*, *23*). The use of Zn^{2+} to grow VP* crystals (after Mn^{2+} treatment) resulted in an intermediate conformation of the metal binding site, where the Glu40 side chain does not occupy the position found in wild-type VP crystals. Mobility of the Glu39 in MnP has been recently shown in some high-resolution crystals, where its side chain occupied two different conformations (*52*). However, the mobility of MnP Glu35 (compared to VP Glu36) is limited by the existence of a salt bridge with Arg177, which is absent in VP, as discussed above.

The variable conformations of VP Glu36 and Glu40 side chains and the high k_{cat} and k_3 values of its E36D and E40D variants, among other results, showed that the VP Mn^{2+} oxidation site, although having the same Mn-coordinating residues as found in MnP, has its own structural and functional peculiarities. This fact, together with the demonstration of long-range electron transfer for oxidation of high redox potential aromatic compounds (*34*, *35*) as previously seen only for LiP (*36*), contributes to the interest of VP as a model ligninolytic peroxidase of biotechnological interest.

ACKNOWLEDGMENT

The use of the protein beamline at the SLS (Villigen, Switzerland) and DESY (Hamburg, Switzerland) synchrotrons is gratefully acknowledged. Andrew T. Smith (Sussex University, U.K.) is acknowledged for critical reading of the manuscript.

SUPPORTING INFORMATION AVAILABLE

One table showing the steady-state kinetic constants of VP* variants (and native VP*) for oxidation of the low-redox potential dye ABTS at high and low efficiency sites. This material is available free of charge via the Internet at http://pubs.acs.org.

REFERENCES

1. Gold, M. H., Youngs, H. L., and Gelpke, M. D. (2000) Manganese peroxidase, *Met. Ions Biol. Syst. 37*, 559−586.
2. Magliozzo, R. S., and Marcinkeviciene, J. A. (1997) The role of Mn(II)-peroxidase activity of mycobacterial catalase-peroxidase in activation of the antibiotic isoniazid, *J. Biol. Chem. 272*, 8867−8870.
3. Muñoz, C., Guillén, F., Martínez, A. T., and Martínez, M. J. (1997) Laccase isoenzymes of *Pleurotus eryngii:* Characterization, catalytic properties and participation in activation of molecular oxygen and Mn^{2+} oxidation, *Appl. Environ. Microbiol. 63*, 2166−2174.
4. Martínez, A. T. (2002) Molecular biology and structure-function of lignin-degrading heme peroxidases, *Enzyme Microb. Technol. 30*, 425−444.
5. Kirk, T. K., and Cullen, D. (1998) Enzymology and molecular genetics of wood degradation by white-rot fungi, in *Environmentally friendly technologies for the pulp and paper industry* (Young, R. A., and Akhtar, M., Eds.) pp 273−308, TAPPI Press, Atlanta, GA.
6. Kirk, T. K., and Farrell, R. L. (1987) Enzymatic "combustion": The microbial degradation of lignin, *Annu. Rev. Microbiol. 41*, 465−505.
7. Lobos, S., Tello, M., Polanco, R., Larrondo, L. F., Manubens, A., Salas, L., and Vicuña, R. (2001) Enzymology and molecular genetics of the ligninolytic system of the basidiomycete *Ceriporiopsis subvermispora*, *Curr. Sci. 81*, 992−997.
8. Martínez, A. T., Camarero, S., Guillén, F., Gutiérrez, A., Muñoz, C., Varela, E., Martínez, M. J., Barrasa, J. M., Ruel, K., and Pelayo, M. (1994) Progress in biopulping of non-woody materials: Chemical, enzymatic and ultrastructural aspects of wheat-straw delignification with ligninolytic fungi from the genus *Pleurotus*, *FEMS Microbiol. Rev. 13*, 265−274.
9. Ruiz-Dueñas, F. J., Camarero, S., Pérez-Boada, M., Martínez, M. J., and Martínez, A. T. (2001) A new versatile peroxidase from *Pleurotus*, *Biochem. Soc. Trans. 29*, 116−122.
10. Ruiz-Dueñas, F. J., Martínez, M. J., and Martínez, A. T. (1999) Molecular characterization of a novel peroxidase isolated from the ligninolytic fungus *Pleurotus eryngii*, *Mol. Microbiol. 31*, 223−236.
11. Camarero, S., Ruiz-Dueñas, F. J., Sarkar, S., Martínez, M. J., and Martínez, A. T. (2000) The cloning of a new peroxidase found in lignocellulose cultures of *Pleurotus eryngii* and sequence comparison with other fungal peroxidases, *FEMS Microbiol. Lett. 191*, 37−43.
12. Moreira, P. R., Duez, C., Dehareng, D., Antunes, A., Almeida-Vara, E., Frère, J. M., Malcata, F. X., and Duarte, J. C. (2005) Molecular characterisation of a versatile peroxidase from a *Bjerkandera* strain, *J. Biotechnol. 118*, 339−352.
13. Heinfling, A., Ruiz-Dueñas, F. J., Martínez, M. J., Bergbauer, M., Szewzyk, U., and Martínez, A. T. (1998) A study on reducing substrates of manganese-oxidizing peroxidases from *Pleurotus eryngii* and *Bjerkandera adusta*, *FEBS Lett. 428*, 141−146.
14. Caramelo, L., Martínez, M. J., and Martínez, A. T. (1999) A search for ligninolytic peroxidases in the fungus *Pleurotus eryngii* involving α-keto-γ-thiomethylbutyric acid and lignin model dimers, *Appl. Environ. Microbiol. 65*, 916−922.
15. Flournoy, D. S., Paul, J. A., Kirk, T. K., and Highley, T. L. (1993) Changes in the size and volume of pores in sweetgum wood during simultaneous rot by *Phanerochaete chrysosporium* Burds, *Holzforschung 47*, 297−301.
16. Bao, W. L., Fukushima, Y., Jensen, K. A., Moen, M. A., and Hammel, K. E. (1994) Oxidative degradation of non-phenolic lignin during lipid peroxidation by fungal manganese peroxidase, *FEBS Lett. 354*, 297−300.
17. Bourbonnais, R., and Paice, M. G. (1990) Oxidation of non-phenolic substrates. An expanded role for laccase in lignin biodegradation, *FEBS Lett. 267*, 99−102.
18. Harvey, P. J., Schoemaker, H. E., and Palmer, J. M. (1986) Veratryl alcohol as a mediator and the role of radical cations in lignin biodegradation by *Phanerochaete chrysosporium*, *FEBS Lett. 195*, 242−246.
19. Glenn, J. K., Akileswaran, L., and Gold, M. H. (1986) Mn(II) oxidation is the principal function of the extracellular Mn-peroxidase from *Phanerochaete chrysosporium*, *Arch. Biochem. Biophys. 251*, 688−696.
20. Poulos, T. L., Edwards, S. L., Wariishi, H., and Gold, M. H. (1993) Crystallographic refinement of lignin peroxidase at 2 Å, *J. Biol. Chem. 268*, 4429−4440.
21. Sundaramoorthy, M., Kishi, K., Gold, M. H., and Poulos, T. L. (1994) The crystal structure of manganese peroxidase from *Phanerochaete chrysosporium* at 2.06-Å resolution, *J. Biol. Chem. 269*, 32759−32767.
22. Harris, R. Z., Wariishi, H., Gold, M. H., and Ortiz de Montellano, P. R. (1991) The catalytic site of manganese peroxidase. Regiospecific addition of sodium azide and alkylhydrazines to the heme group, *J. Biol. Chem. 266*, 8751−8758.
23. Sundaramoorthy, M., Kishi, K., Gold, M. H., and Poulos, T. L. (1997) Crystal structures of substrate binding site mutants of manganese peroxidase, *J. Biol. Chem. 272*, 17574−17580.
24. Kusters-van Someren, M., Kishi, K., Lundell, T., and Gold, M. H. (1995) The manganese binding site of manganese peroxidase: Characterization of an Asp179Asn site-directed mutant protein, *Biochemistry 34*, 10620−10627.
25. Kishi, K., Kusters-van Someren, M., Mayfield, M. B., Sun, J., Loehr, T. M., and Gold, M. H. (1996) Characterization of manganese(II) binding site mutants of manganese peroxidase, *Biochemistry 35*, 8986−8994.
26. Gelpke, M. D. S., Moënne-Loccoz, P., and Gold, M. H. (1999) Arginine 177 is involved in Mn(II) binding by manganese peroxidase, *Biochemistry 38*, 11482−11489.

27. Gelpke, M. D. S., Youngs, H. L., and Gold, M. H. (2000) Role of arginine 177 in the Mn^{II} binding site of manganese peroxidase. Studies with R177D, R177E, R177N, and R177Q mutants, *Eur. J. Biochem. 267*, 7038−7045.
28. Whitwam, R. E., Brown, K. R., Musick, M., Natan, M. J., and Tien, M. (1997) Mutagenesis of the Mn^{2+}-binding site of manganese peroxidase affects oxidation of Mn^{2+} by both compound I and compound II, *Biochemistry 36*, 9766−9773.
29. Mester, T., and Tien, M. (2001) Engineering of a manganese-binding site in lignin peroxidase isozyme H8 from *Phanerochaete chrysosporium*, *Biochem. Biophys. Res. Commun. 284*, 723−728.
30. Wilcox, S. K., Putnam, C. D., Sastry, M., Blankenship, J., Chazin, W. J., McRee, D. E., and Goodin, D. B. (1998) Rational design of a functional metalloenzyme: Introduction of a site for manganese binding and oxidation into a heme peroxidase, *Biochemistry 37*, 16853−16862.
31. Yeung, B. K. S., Wang, X. T., Sigman, J. A., Petillo, P. A., and Lu, Y. (1997) Construction and characterization of a manganese-binding site in cytochrome *c* peroxidase: Towards a novel manganese peroxidase, *Chem. Biol. 4*, 215−221.
32. Banci, L., Camarero, S., Martínez, A. T., Martínez, M. J., Pérez-Boada, M., Pierattelli, R., and Ruiz-Dueñas, F. J. (2003) NMR study of Mn(II) binding by the new versatile peroxidase from the white-rot fungus *Pleurotus eryngii*, *J. Biol. Inorg. Chem. 8*, 751−760.
33. Pérez-Boada, M., Doyle, W. A., Ruiz-Dueñas, F. J., Martínez, M. J., Martínez, A. T., and Smith, A. T. (2002) Expression of *Pleurotus eryngii* versatile peroxidase in *Escherichia coli* and optimisation of *in vitro* folding, *Enzyme Microb. Technol. 30*, 518−524.
34. Pogni, R., Baratto, M. C., Teutloff, C., Giansanti, S., Ruiz-Dueñas, F. J., Choinowski, T., Piontek, K., Martínez, A. T., Lendzian, F., and Basosi, R. (2006) A tryptophan neutral radical in the oxidized state of versatile peroxidase from *Pleurotus eryngii*: a combined multi-frequency EPR and DFT study, *J. Biol. Chem. 281*, 9517−9526.
35. Pérez-Boada, M., Ruiz-Dueñas, F. J., Pogni, R., Basosi, R., Choinowski, T., Martínez, M. J., Piontek, K., and Martínez, A. T. (2005) Versatile peroxidase oxidation of high redox potential aromatic compounds: Site-directed mutagenesis, spectroscopic and crystallographic investigations of three long-range electron transfer pathways, *J. Mol. Biol. 354*, 385−402.
36. Doyle, W. A., Blodig, W., Veitch, N. C., Piontek, K., and Smith, A. T. (1998) Two substrate interaction sites in lignin peroxidase revealed by site-directed mutagenesis, *Biochemistry 37*, 15097−15105.
37. Weiner, M. P., Costa, G. L., Schoettlin, W., Cline, J., Mathur, E., and Bauer, J. C. (1994) Site-directed mutagenesis of double-stranded DNA by the polymerase chain reaction, *Gene 151*, 119−123.
38. Sambrook, J., and Russell, D. W. (2001) *Molecular cloning*, CSHL Press, Cold Spring Harbor, NY.
39. Laemmli, U. K. (1970) Cleavage of structural proteins during the assembly of the head of bacteriophage T_4, *Nature 227*, 680−685.
40. Martínez, M. J., Ruiz-Dueñas, F. J., Guillén, F., and Martínez, A. T. (1996) Purification and catalytic properties of two manganese-peroxidase isoenzymes from *Pleurotus eryngii*, *Eur. J. Biochem. 237*, 424−432.
41. Kabsch, W. (1993) Automatic processing of rotation diffraction data from crystals of initially unknown symmetry and cell constants, *J. Appl. Crystallogr. 26*, 795−800.
42. Navaza, J. (1994) Amore—An automated package for molecular replacement, *Acta Crystallogr. A 50*, 157−163.
43. Collaborative Computational Project No. 4 (1994) The CCP4 suite: programs from protein crystallography, *Acta Crystallogr. D 50*, 760−763.
44. Hatakka, A. (1994) Lignin-modifying enzymes from selected white-rot fungi—Production and role in lignin degradation, *FEMS Microbiol. Rev. 13*, 125−135.
45. Hildén, K., Martínez, A. T., Hatakka, A., and Lundell, T. (2005) The two manganese peroxidases Pr-MnP2 and Pr-MnP3 of *Phlebia radiata*, a lignin-degrading basidiomycete, are phylogenetically and structurally divergent, *Fungal Genet. Biol. 42*, 403−419.
46. Stewart, P., Whitwam, R. E., Kersten, P. J., Cullen, D., and Tien, M. (1996) Efficient expression of a *Phanerochaete chrysosporium* manganese peroxidase gene in *Aspergillus oryzae*, *Appl. Environ. Microbiol. 62*, 860−864.
47. Pease, E. A., Aust, S. D., and Tien, M. (1991) Heterologous expression of active manganese peroxidase from *Phanerochaete chrysosporium* using the baculovirus expression system, *Biochem. Biophys. Res. Commun. 179*, 897−903.
48. Whitwam, R. E., Gazarian, I. G., and Tien, M. (1995) Expression of fungal Mn peroxidase in *E. coli* and refolding yield active enzyme, *Biochem. Biophys. Res. Commun. 216*, 1013−1017.
49. Ambert-Balay, K., Dougherty, M., and Tien, M. (2000) Reactivity of manganese peroxidase: Site-directed mutagenesis of residues in proximity to the porphyrin ring, *Arch. Biochem. Biophys. 382*, 89−94.
50. Youngs, H. L., Gelpke, M. D. S., Li, D. M., Sundaramoorthy, M., and Gold, M. H. (2001) The role of Glu39 in Mn-II binding and oxidation by manganese peroxidase from *Phanerochaete chrysosporium*, *Biochemistry 40*, 2243−2250.
51. Maeda, Y., Kajiwara, S., and Ohtaguchi, K. (2001) Manganese peroxidase gene of the perennial mushroom *Elfvingia applanata*: cloning and evaluation of its relationship with lignin degradation, *Biotechnol. Lett. 23*, 103−109.
52. Sundaramoorthy, M., Youngs, H. L., Gold, M. H., and Poulos, T. L. (2005) High-resolution crystal structure of manganese peroxidase: substrate and inhibitor complexes, *Biochemistry 44*, 6463−6470.
53. Gelpke, M. D. S., Sheng, D., and Gold, M. H. (2000) Mn^{II} is not a productive substrate for wild-type or recombinant lignin peroxidase isozyme H2, *Arch. Biochem. Biophys. 381*, 16−24.

BI061542H